Volume 16
Number 4
April 1977

Inorganic Chemistry

Contribution from the School of Chemical Sciences,
University of Illinois, Urbana, Illinois 61801

Preparation and Physical Properties of Oxidation Products of Oxo-Bridged Binuclear Iron(III) Complexes. Mixed-Valence Diiron(III,IV) Complexes

RONALD G. WOLLMANN and DAVID N. HENDRICKSON*[1]

Received July 14, 1976 AIC605058

The chemical oxidation of μ-oxo-bis(tetraphenylporphinatoiron(III)), $[Fe(TPP)]_2O$, and μ-oxo-bis(*N*,*N*′-ethylenebis(salicylideniminato)iron(III)), $[Fe(salen)]_2O$, to mixed-valence $Fe^{III}Fe^{IV}$ compounds of the composition $[Fe_2(L)_2O]X$ (X^- is variously PF_6^-, BF_4^-, ClO_4^-, or I_3^-) is reported. An antiferromagnetic exchange interaction is indicated by variable-temperature (4.2–267 K) magnetic susceptibility data, which can be least-squares fit to the theoretical equations for an isotropic exchange interaction ($\hat{H} = -2J\hat{S}_1\cdot\hat{S}_2$) in an $S_1 = {}^5/_2$, $S_2 = 2$ dimer. The exchange parameters, J, for the $[Fe_2(salen)_2O]X$ compounds are in the range of −7.5 to −17.6 cm^{-1}. Inclusion of axial zero-field splitting, $D\hat{S}_Z^2$, into the theory for the porphyrin $[Fe_2(TPP)_2O]X$ compounds yields J values in the range of −82.5 to −119 cm^{-1} and $|D|$ values in the range of 11.7–19.9 cm^{-1}. X-Band (6–300 K) and Q-band (110–300 K) EPR, ^{57}Fe Mössbauer (4.2–80 K), infrared (30–300 K), and electronic absorption spectroscopic data are also presented. No asymmetric Fe–O–Fe band is observed in the IR spectrum of any of the compounds. No intervalence-transfer bands can be identified in the room-temperature solution electronic absorption spectra of $[Fe_2(TPP)_2O]X$. Electronic absorptions are observed at 450–510 nm in the spectra of the $[Fe_2(salen)_2O]X$ compounds and these are tentatively assigned as intervalence-transfer bands. A single, temperature-independent, quadrupole-split doublet is observed in the Mössbauer spectra for all of the compounds. The thermal intervalence electron-transfer rates are greater than $\sim 10^7$ s^{-1} for all compounds. Isotropic EPR signals with g values of ~2.0 are observed for the $[Fe_2(salen)_2O]X$ compounds; temperature-dependent line widths indicate that the thermal electron-transfer rates are greater than $\sim 10^{10}$ s^{-1} for these $Fe^{III}Fe^{IV}$ compounds. Either a high-spin Fe(III) EPR signal or no EPR signal is observed for $[Fe_2(TPP)_2O]X$ and this indicates that the thermal rates are $\lesssim 10^{10}$ s^{-1} for these diiron(III,IV) porphyrin compounds.

Introduction

The intimate involvement of iron porphyrins in biologically active molecules has stimulated intensive investigations of various iron complexes in recent years. Several metalloproteins are now known to have iron heme units in close proximity, e.g., cytochrome *c* oxidase[2] and cytochromes c_3.[3] Many of the cytochrome c_3 proteins have molecular weights of 13 000 and four heme units. A model has been proposed[4] wherein the four heme groups form a box with two pairs of hemes roughly planar to each other and about 10 Å apart. The cytochrome c_3 proteins are, of course, integral parts of electron-transport chains. It is thus interesting that, despite the relatively close 10-Å separation of hemes within this protein, there is relatively slow electron exchange between the hemes. A better understanding of the factors influencing electron exchange (transfer) between iron porphyrin centers is needed and in this paper we report on our efforts to study thermal electron transfer in $Fe^{III}Fe^{IV}$ dimers derived from μ-oxo-bridged Fe(III) dimers.

The considerable work on μ-oxo-bridged ferric dimers has been reviewed.[5] It is believed that, in solution, the dimeric intermediates and equilibria associated with the formation of such μ-oxo dimers are numerous.[6] This has been indicated by a study of the rapid incorporation of ^{18}O into the Fe–O–Fe unit from $^{18}OH_2$ solvent. In addition, kinetic investigations of the breakdown of Fe–O–Fe units have indicated the possible existence of dihydroxo- and aquohydroxo-bridged dimeric intermediates.[7] Single-crystal x-ray structures have established the existence of dihydroxo-[8] and dialkoxo-bridged[9] dimeric complexes. Because we are interested in mixed-valence-state compounds,[10] we were intrigued by the report of a synthesis of two apparently mixed-valent μ-oxo-diiron(III,IV) porphyrins.[11] These complexes offer an opportunity to study electron transfer between porphyrin iron ions and, as such, it was our intent to provide a detailed characterization of this type of $Fe^{III}Fe^{IV}$ dimer. In this work, we report on the one-electron oxidation products obtained from μ-oxo-bis(tetraphenylporphyrinatoiron(III)) and μ-oxo-bis(*N*,*N*′-ethylenebis(salicylideniminato)iron(III)).

Experimental Section

Compound Preparation. Analytical reagent grade chemicals were used in this work and all analytical data were obtained from the Microanalytical Laboratory of the School of Chemical Sciences. *meso*-Tetraphenylporphyrin (TPP) was synthesized as previously reported.[12]

The preparation of **μ-oxo-bis(tetraphenylporphyrinatoiron(III))**, $[Fe(TPP)]_2O$, has been reported.[13] The reaction of Fe(TPP)X, X = halide or acetate, with hydroxide ion followed by chromatography gives low yields (20–30%) of $[Fe(TPP)]_2O$. In this work, we developed an improved high-yield (~90%) synthesis of $[Fe(TPP)]_2O$ based on the autoxidation[14] of Fe(TPP). In this synthesis, unless otherwise stated, all reactions were carried out under a nitrogen atmosphere using Schlenk-type apparatus. All solvents were purged with nitrogen gas before use. Glacial acetic acid (500 mL) was brought to reflux

temperature in a 1-L two-necked round-bottom flask equipped with a Schlenk filtration tube. Iron powder (1 g) was placed in the acetic acid and allowed to react for 2–3 h. The resulting ferrous acetate solution was then filtered through the Schlenk tube. In a 1-L two-necked round-bottom flask, 2 g of TPP was dissolved in a solution of $CHCl_3$ (200 mL) and pyridine (80 mL) and then the mixture was brought to reflux temperature. The ferrous acetate solution was transferred, via syringe needle and plastic tubing, into the TPP solution. Purple microcrystals formed immediately upon addition. The mixture was stirred for 2–3 h, cooled, and filtered. The purple crystalline solid was washed with methanol (100 mL) and dried thoroughly with a nitrogen stream. The dry solid was dissolved in hot benzene (400 mL) and evaporated to dryness *in the air*. The resulting purple powder was recrystallized from $CHCl_3$ to yield $[Fe(TPP)]_2O$ (2 g, 91% yield). Anal. Calcd for $C_{88}H_{56}N_8Fe_2O$: C, 78.10; H, 4.18; N, 8.28; Fe, 8.25. Found: C, 78.06; H, 4.32; N, 8.10; Fe, 7.66.

A sample of μ-oxo-bis(*N*,*N*'-ethylenebis(salicylideniminato)-iron(III)), $[Fe(salen)]_2O$, was prepared by a previously described method[15] and recrystallized from CH_2Cl_2. Anal. Calcd for $C_{32}H_{28}N_4O_5Fe_2$: C, 58.20; H, 4.28; N, 8.48; Fe, 16.92. Found: C, 57.93; H, 4.16; N, 8.48; Fe, 16.72.

Samples of **$[Fe_2(TPP)_2O]PF_6$** were prepared by two methods. **Method I.** $[Fe(TPP)]_2O$ (0.1 g) was dissolved in $CHCl_3$ (20 mL) and an excess of solid $NOPF_6$ was added to the solution with stirring. The solution was stirred for an additional 30 min and then evaporated to dryness. The resulting solid was washed with H_2O and dried in vacuo over P_4O_{10}. Anal. Calcd for $[C_{88}H_{56}N_8Fe_2O]PF_6$: C, 70.54; H, 3.78; N, 7.48; Fe, 7.46. Found: C, 69.24; H, 3.74; N, 7.36; Fe, 7.28. **Method II.** $[Fe(TPP)]_2O$ (0.2 g) was dissolved in refluxing $CHCl_3$ (20 mL) and 5 drops of aqueous HPF_6 (60–65%) were added to the solution with stirring. The solution was stirred for an additional 10 min and then evaporated to dryness. The resulting solid was washed with H_2O and dried in vacuo over P_4O_{10}. In this method O_2 is probably the oxidizing agent; ferrocenes are oxidized by O_2 in the presence of relatively strong acids.[10] Anal. Found for $[C_{88}H_{56}N_8Fe_2O]PF_6$: C, 68.58; H, 3.99; N, 7.14; Fe, 6.91.

Samples of **$[Fe_2(TPP)_2O]BF_4$** were prepared as in method II above using (50%) aqueous HBF_4. Anal. Calcd for $[C_{88}H_{56}N_8Fe_2]BF_4$: C, 73.39; H, 3.93; N, 7.78; Fe, 7.76; B, 0.75. Found: C, 73.06; H, 3.88; N, 7.75; Fe, 7.55; B, 0.64. Molecular weight: calcd, 1440.03; found, 716 (in $CHCl_3$).

$[Fe_2(salen)_2O]X$ ($X^- = PF_6^-, ClO_4^-$). One gram of $[Fe(salen)]_2O$ was dissolved in 300 mL of refluxing $CHCl_3$. The appropriate solid NO^+X^- was added and the mixture was stirred for 15 min, during which time a reddish purple precipitate formed. The mixture volume was reduced to 100 mL, cooled, and filtered. The solid was washed with Et_2O (100 mL) and dried in vacuo over P_4O_{10}. Anal. Calcd for $[C_{32}H_{28}N_4O_5Fe_2]PF_6$: C, 47.73; H, 3.51; N, 6.96; Fe, 13.87; mol wt 805.31. Found: C, 49.25; H, 3.79; N, 7.22; Fe, 13.74; effective mol wt in acetone 872. Calcd for $[C_{32}H_{28}N_4O_5Fe]ClO_4$: C, 50.58; H, 3.72; N, 7.37; Fe, 14.70; mol wt 759.76. Found: C, 50.16; H, 4.20; N, 7.41; Fe, 14.00; mol wt in acetone 739.

$[Fe_2(salen)_2O]BF_4$. $[Fe(salen)]_2O$ (0.5 g) was dissolved in a refluxing solution of $CHCl_3$ (150 mL) and benzene (150 mL). Five drops of HBF_4 (aqueous, 50%) were added to the solution with rapid stirring. The solution was stirred for 15 min, during which time a reddish precipitate formed. The mixture was filtered, washed with Et_2O to remove excess HBF_4, and dried in vacuo over P_4O_{10}. Anal. Calcd for $[C_{32}H_{28}N_4O_5Fe]BF_4$: C, 51.44; H, 3.79; N, 7.50; Fe, 14.95. Found: C, 52.40; H, 3.89; N, 7.51; Fe, 15.22.

$[Fe_2(salen)_2O]I_3 \cdot CHCl_3$. A saturated solution of $[Fe(salen)]_2O$ and a saturated $CHCl_3$ solution of I_2 were placed in two compartments of a U-tube having two compartments separated by a medium-porosity sintered-glass frit. After several days, the reddish brown microcystalline precipitate was collected, washed with $CHCl_3$, and dried in vacuo over P_4O_{10}. Anal. Calcd for $[C_{32}H_{28}N_4O_5Fe_2]I_3 \cdot CHCl_3$: C, 34.16; H, 2.52; N, 4.83; Fe, 9.63; I, 32.81; Cl, 9.17. Found: C, 34.02; H, 2.77; N, 4.93; Fe, 9.39; I, 34.56; Cl, 8.24.

Physical Measurements. Infrared spectra were recorded on Perkin-Elmer Model 457 and 467 spectrophotometers. Samples were prepared as 13-mm KBr pellets. Low-temperature IR spectra were obtained using a Cryogenics Technology, Inc., "Spectrim" closed-cycle helium gas refrigerator with the cryocooling head equipped with KBr windows (50 × 4 mm).

Variable-temperature (4.2–267 K) magnetic susceptibility data were obtained with a PAR Model 150A vibrating-sample magnetometer. A calibrated GaAs temperature-sensitive diode was used to monitor the temperature in conjunction with a $CuSO_4 \cdot 5H_2O$ standard.

Iron-57 Mössbauer spectra were obtained at 4.2 K on an instrument previously described.[16] Spectra at liquid nitrogen temperatures were obtained with a second instrument.[17]

Electron paramagnetic resonance spectra were obtained with Varian E-line spectrometers using an E101 microwave bridge with a 6-in. (10 kG) magnet for X-band measurements and an E110 microwave bridge with a 12-in. (25 kG) magnet for Q-band measurements. X-Band measurements at 90 ± 10 K were obtained by using a Varian liquid nitrogen cavity insert and at 8 ± 2 K by using an Air Products Heli-tran liquid-helium cooling system. Temperatures were determined by employing an Ohmite 2.7 ± 10% kΩ ($^1/_4$ W) carbon resistor. The low-temperature of the Q-band measurements was estimated to be ~110 K and this low temperature was achieved by surrounding the cavity with a glass dewar and passing liquid nitrogen cooled gaseous nitrogen through the system.

Electronic absorption spectra were run on a Cary 14 spectrophotometer using quartz cells of 1-cm path length.

Computer fittings of magnetic susceptibility data were carried out with an adapted version of the function-minimization program known as STEPT.[18] Computer fittings of ^{57}Fe Mössbauer data to Lorenztian lines were carried out with a modified version of a previously reported program.[19]

Results

Electrochemical work[11] on $[Fe(TPP)]_2O$, which we duplicated in this study, showed two one-electron half-waves at 0.84 and 1.09 V vs. an aqueous saturated calomel. We have carried out differential-pulse polarographic and cyclic voltammetric measurements on $[Fe(salen)]_2O$ dissolved in CH_2Cl_2 with platinum electrodes and *n*-butylammonium perchlorate as supporting electrolyte. It appears that the salen dimer also shows two oxidation waves at a voltage less than 1.2 V, but the half-wave positions cannot be properly assessed because the waves are poorly resolved and ill defined due to adsorption onto the electrode surface. Dc polarographic measurements on either $[Fe(TPP)]_2O$ or $[Fe(salen)]_2O$ did not yield well-resolved plateaus.

The difference in electrochemical characteristics of $[Fe(salen)]_2O$ and $[Fe(TPP)]_2O$ parallels our observations (see Experimental Section) that the $[Fe_2(salen)_2O]X$ compounds precipitate out of solution ($CHCl_3$ or CH_2Cl_2) whereas $[Fe_2(TPP)_2O]X$ is somewhat soluble in these organic solvents. Unoxidized $[Fe(TPP)]_2O$ and $[Fe(salen)]_2O$ are insoluble in water and diethyl ether, very slightly soluble in acetone and ethanol, and soluble in organic solvents such as chloroform and benzene. The $[Fe_2(TPP)_2O]X$ compounds are also insoluble in water but are more soluble than the unoxidized compound in diethyl ether, acetone, and chloroform. On the other hand, oxidation of the salen dimer results in more dramatic changes in solubility. The $[Fe_2(salen)_2O]X$ compounds are very slightly soluble in chloroform, diethyl ether, and benzene. They are quite soluble in water, ethanol, and acetone.

Water, ethanol, and acetone solutions of the $[Fe_2(salen)_2O]X$ compounds are orange-red to red. If these solutions are allowed to stand for periods of about 1 day, a red-brown powder begins to form. This powder is most certainly the unoxidized dimer. The tendency to decompose in solution has frustrated all of our attempts to grow crystals. Previous workers have reported that methylene chloride solutions of singly oxidized oxo-bridged iron porphyrins decay to the unoxidized material at the rate of a few percent per hour.[11]

$[Fe_2(salen)_2O]X$. Nitrosonium salts, NOX, are very convenient oxidizing agents.[20] The $X^- = PF_6^-$ and ClO_4^- compounds of salen were prepared with $NOPF_6$ and $NOClO_4$, respectively, while the $X^- = BF_4^-$ salt was prepared by oxidation with aqueous HBF_4. A microcrystalline compound with the composition $[Fe_2(salen)_2O]I_3 \cdot CHCl_3$ resulted from iodine oxidation of the μ-oxo dimer dissolved in chloroform. Effective

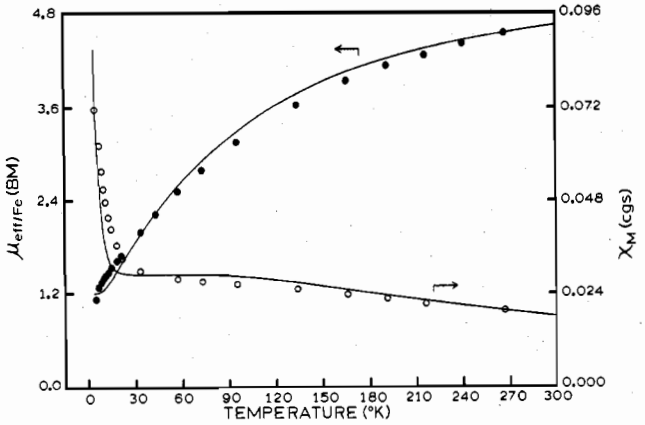

Figure 1. Molar paramagnetic susceptibility in cgsu and effective magnetic moment per iron in μ_B vs. temperature curves for $[Fe_2(salen)_2O]PF_6$. The solid lines result from least-squares fitting of the data to the $S_1 = {}^5/_2$, $S_2 = 2$ dimer equation including the interdimer interaction parameter $Z'J'$ with $g = 2.0$ (no TIP included).

molecular weight determinations were carried out for acetone solutions of $[Fe_2(salen)_2O]PF_6$ and $[Fe_2(salen)_2O]ClO_4$ using vapor pressure osmometry. The observed effective molecular weights were found to be 872 and 739, respectively. These values correspond to the actual molecular weights (805.31 and 759.76, respectively) rather than to half the actual values, as expected for a 1:1 electrolyte. Apparently, there is ion pairing in acetone. As such, ethanol was selected as a solvent and conductivity measurements were carried out for ethanol solutions of $[Fe_2(salen)_2O]ClO_4$. A linear plot of conductivity vs. the square root of the concentration was obtained in the concentration range of $3.0–5.0 \times 10^{-4}$ M. The slope of this line was found to be 357 Ω^{-1} $M^{-1/2}$. Similar plots were obtained for NH_4PF_6 and $CaCl_2 \cdot 2H_2O$ in ethanol over the same concentration range; the slopes were found to be 437 and 933 Ω^{-1} $M^{-1/2}$, respectively. Previous work has shown that a comparison of the variation of the equivalent conductance as a function of concentration of a particular compound, relative to known electrolytes, is sufficient to determine the type of electrolyte.[21] Thus, $[Fe_2(salen)_2O]ClO_4$ is clearly a 1:1 electrolyte; the somewhat smaller value of 357 Ω^{-1} $M^{-1/2}$ relative to the 437 Ω^{-1} $M^{-1/2}$ value for the known 1:1 electrolyte is probably indicative of a small amount of ion pairing even in ethanol.

Evidence for the presence of dimers in $[Fe_2(salen)_2O]X$ can be found in our magnetic susceptibility measurements carried out in the range of 4.2–267 K. All of the compounds gave data characteristic of antiferromagnetic exchange interactions. The effective magnetic moments (μ_{eff}) at 267 K were found to be 4.52, 3.78, 4.37, and 4.09 μ_B for $[Fe_2(salen)_2O]PF_6$, $[Fe_2(salen)_2O]ClO_4$, $[Fe_2(salen)_2O]BF_4$, and $[Fe_2(salen)_2O]I_3 \cdot CHCl_3$, respectively. As the temperature was decreased to 4.2 K, the magnetic moments smoothly decreased to values of 1.09, 0.80, 0.72, and 0.51 μ_B, respectively. Typical data for $[Fe_2(salen)_2O]PF_6$ are illustrated in Figure 1 and are summarized in Table I. Data for the other compounds can be found in the supplementary material. From other evidence (vide infra), it is clear that the temperature dependence of μ_{eff} is due to an antiferromagnetic exchange interaction and not to some other effect such as a high-spin, low-spin equilibrium.

An isotropic exchange interaction for a dimeric complex is handled with a spin Hamiltonian, $\hat{H} = -2J\hat{S}_1 \cdot \hat{S}_2$, where J is the *intra*dimer exchange parameter and $\hat{S}_1$ and $\hat{S}_2$ are the spin operators for metal centers 1 and 2, respectively. For the case of an $Fe^{III}Fe^{IV}$ dimer, $S_1 = {}^5/_2$ and $S_2 = 2$, and equations have been derived by Wojciechowski for the magnetic susceptibility of such an exchange-interacting dimer.[22] With no account given to single-ion zero-field interactions and by using perturbation theory to second order, the molar paramagnetic susceptibility for this type of dimer is given as

$$\chi_M = (Ng^2\beta^2/kT)\frac{1/2A + 5B + 35C/2 + 42D + 165/2}{2A + 4B + 6C + 8D + 10}$$

In this expression, N, g, β, k, and T have their usual meanings and the various exponential terms are found to be $A = \exp(-24J/kT)$, $B = \exp(-21J/kT)$, $C = \exp(-16J/kT)$, $D = \exp(-9J/kT)$.

Similar equations were also derived by Wojciechowski[23] for the case of an isotropic exchange interaction in a $Fe^{III}Fe^{III}$ dimer where $S_1 = S_2 = {}^5/_2$. Computer programs were written to least-squares fit the data to either model. Very poor fits to the data sets were obtained for each of the $[Fe_2(salen)_2O]X$ compounds when the $S_1 = S_2 = {}^5/_2$ theoretical equation was used. This is simply a reflection of the fact that an even-spin system, where $S_1 = S_2 = {}^5/_2$, has a diamagnetic ($S' = 0$) ground state when $J < 0$, and if an appreciable exchange interaction is present, as indicated by a low μ_{eff} value at room temperature, then the effective moment is expected to go to a very small value at low temperatures.

In Figure 1, it can be seen that the value of μ_{eff} per iron ion decreases only to ~ 1.1 μ_B at 4.2 K. This is an appropriate value for *one unpaired electron per two iron ions* ($1.73/2^{1/2} \simeq 1.2$ μ_B). Thus, is was no surprise that better fits were obtained with the above susceptibility equation for an $S_1 = {}^5/_2$, $S_2 = 2$ dimer. There was still a small deviation in the fitting of the low-temperature data to this theoretical model. A weak *inter*dimer exchange Hamiltonian is represented by $-2Z'J'\hat{S}_Z'\langle S_Z'\rangle$ where Z' is the cluster lattice coordination number, J' is the *inter*dimer exchange parameter, and $\hat{S}_Z'$ is the quantized spin operator for the *total* dimer spin. In a manner similar to that described previously,[24] a term in the parameter $Z'J'$ (taken together as one parameter) was incorporated into the above $S_1 = {}^5/_2$, $S_2 = 2$ equation. The least-squares fit of the data (points) for $[Fe_2(salen)_2O]PF_6$, illustrated in Figure 1 as lines, is very reasonable. We assumed $g = 2$ in fitting the data for all of the $[Fe_2(salen)_2O]PF_6$ compounds. The fitting parameters, J and $Z'J'$, are given in Table II, where it can be seen that, for these salen compounds, the J values range from -17.6 to -7.5 cm^{-1}. It must be emphasized that we found that the inclusion of the $Z'J'$ parameter did not appreciably affect the J values obtained. A theoretical model (see Appendix) including single-ion zero-field interactions (necessary for the TPP dimers) was also

Table I. Magnetic Susceptibility Data for $[Fe_2(salen)_2O]PF_6$[a]

	$10^3\chi_M$, cgsu		μ_{eff}/Fe, μ_B	
T, K	Obsd	Calcd	Obsd	Calcd
267	19.19	19.57	4.52	4.57
240	20.13	20.83	4.40	4.47
216	20.89	22.10	4.25	4.37
192	22.13	23.46	4.12	4.24
166	23.22	24.98	3.92	4.07
134	24.57	26.83	3.62	3.78
94.5	25.87	28.54	3.13	3.29
72.5	26.52	29.00	2.77	2.90
56.9	27.34	29.05	2.49	2.57
42.7	28.35	28.99	2.20	2.23
33.0	29.51	28.97	1.97	1.96
20.6	33.93	29.50	1.67	1.56
17.7	36.21	30.13	1.60	1.46
14.3	40.19	31.91	1.52	1.35
12.3	43.19	34.15	1.46	1.30
10.5	47.26	37.66	1.41	1.26
9.4	50.49	40.92	1.38	1.24
7.9	55.22	47.45	1.32	1.22
6.4	61.84	57.75	1.26	1.22
4.2	71.30	86.83	1.09	1.21

[a] The diamagnetic correction used is -363×10^{-6} cgsu/mol.

Table II. Magnetic Susceptibility Parameters

Compd	J, cm^{-1}	$Z'J'$, K	$\|D\|$, cm^{-1}	$g_{\parallel}$	$g_{\perp}$
$[Fe(salen)]_2O^+PF_6^-$	−11.6	−0.05			
$[Fe(salen)]_2O^+ClO_4^-$	−17.6	−1.6			
$[Fe(salen)]_2O^+BF_4^-$	−8.7	−2.3			
$[Fe(salen)]_2O^+I_3^-\cdot CHCl_3$	−7.5	−5.9			
$(FeTPP)_2O^+PF_6^-$	−119		11.7	2.34	5.47
$(FeTPP)_2O^+BF_4^-$	−82.5		19.9	3.11	4.80

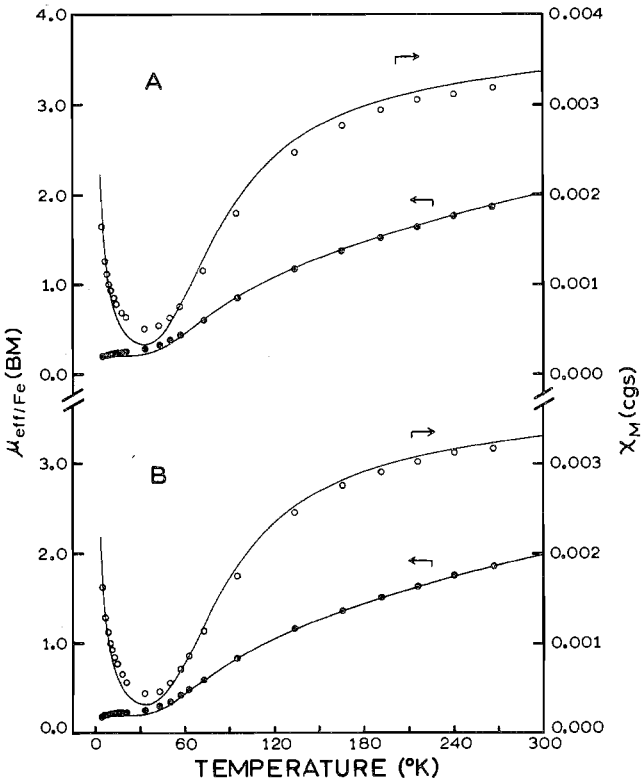

Figure 2. Molar paramagnetic susceptibilities in cgsu and effective moments per iron in μ_B vs. temperature curves for (A) $[Fe(salen)]_2O$ and (B) $[Fe(1,2\text{-PS})]_2O$. The solid lines result from least-squares fitting of the data to the $S_1 = S_2 = {}^5/_2$ dimer equation including an ~2% high-spin ferric impurity.

tried on the salen data and it resulted in essentially the same J values (and negligibly small single-ion zero-field splitting parameters).

An earlier report[25] has shown that the presence of high-spin Fe(III) impurities can influence the determination of J values in μ-oxo-bridged Fe(III) dimers and that the amount of impurities can be evaluated by measuring the magnetic susceptibilities to temperatures at or near 4.2 K. Susceptibility data for $[Fe(salen)]_2O$ have only been recorded[15,26] down to liquid nitrogen temperatures to give $J = -95$ cm^{-1}. It was thought that it would be useful to have magnetic susceptibility data down to 4.2 K for $[Fe(salen)]_2O$ and one very similar compound, $[Fe(1,2\text{-PS})]_2O$, where 1,2-PS is 1,2-propylenebis(salicylideniminate). The effective magnetic moments (per iron ion) for both of these compounds at 267 K were found to be 1.83 μ_B, which decreased to 0.16 μ_B at 4.2 K. As can be seen in Figure 2, the susceptibility curves for these two compounds do show the presence of some small amount of paramagnetic impurities. That is, below ~20 K, the susceptibility increases as the temperature decreases. The data were fit to the perturbation equations for isotropic exchange in a ferric dimer, $S_1 = S_2 = {}^5/_2$. Exchange parameters of −89 and −91 cm^{-1} were obtained for $[Fe(salen)]_2O$ and $[Fe(1,2\text{-PS})]_2O$, respectively. Previous work[15,26] gave $J = -95$ cm^{-1} for the former compound. We find with our least-squares fitting that the paramagnetic impurities are less than 2% for both compounds (assuming that the impurity is a high-spin Fe(III) species).

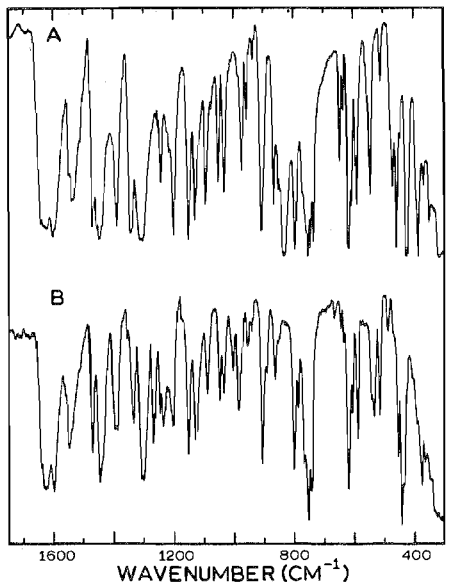

Figure 3. The 30-K IR spectra of (A) $[Fe(salen)]_2O$ and (B) $[Fe_2(salen)_2O]I_3\cdot CHCl_3$, run as KBr pellets.

Variable-temperature (30–300 K) infrared spectra were obtained for $[Fe(salen)]_2O$ and the oxidation compounds. At room temperature, the asymmetric Fe–O–Fe stretching band which is located at 832 cm^{-1} for the oxo-bridged Fe(III) dimer is not seen in the spectra of the oxidation compounds. It was hoped that low-temperature IR spectra would provide a resolution improved to such a degree as to allow an identification of a shifted Fe–O–Fe band. The 30-K, KBr-pellet IR spectra of $[Fe(salen)]_2O$ and $[Fe_2(salen)_2O]I_3\cdot CHCl_3$ are illustrated in Figure 3. The spectrum of the latter compound is typical of the oxidation compounds. A comparison of the two spectra in Figure 3 shows that, even with the improved resolution at 30 K, there is no reasonably strong band in the triiodide spectrum that can be taken as a shifted Fe–O–Fe band. It is also evident that there is a marked decrease in the intensity of two bands at 649 and 637 cm^{-1} relative to the unoxidized dimer. Furthermore, close inspection reveals that many of the peaks which have been assigned[27,28] to ligand vibrations shift to higher energies by 5–15 cm^{-1} in going from the unoxidized to the oxidized compounds. Aside from these differences, the spectra of the unoxidized and oxidized dimers are very similar.

The presence of a band in the 800–900-cm^{-1} region has been used to characterize oxo-bridged iron(III) complexes.[5] No comments about the presence or absence of an asymmetric Fe–O–Fe band were made in the previous investigation of the two oxidized μ-oxo-diiron(III,IV) porphyrins, even though solid compounds such as $[Fe_2(TPP)_2O]ClO_4$ were prepared.[11] A recent single-crystal x-ray structure analysis of an oxo-bridged Mn(III) complex has unequivocally established the presence of an oxo bridge.[29] However, the IR spectrum of this compound was reported not to show a strong band assignable to the asymmetric Mn–O–Mn stretch. An extremely weak peak at 880 cm^{-1} was tentatively assigned to this vibration, but the possibility that this band is due to an impurity was not eliminated. It is very interesting to note that an oxo-centered trinuclear iron(III) acetate shows an asymmetric Fe_3O stretch at 530 cm^{-1}, which loses considerable intensity and shifts to higher energies by 3–8 cm^{-1} upon reduction of the complex to the mixed-valence oxo-centered $Fe^{III}_2Fe^{II}$ trinuclear complex.[30] In view of these observations, it is entirely possible that a weak-intensity Fe–O–Fe band could be shifted in position and obscured by ligand vibrations in the $[Fe_2(sal-$

Table III. Mössbauer Parameters

Compd	δ,[a,b] mm/s		ΔE_Q,[b] mm/s		Γ,[b,c] mm/s	
	80 K	4.2 K	80 K	4.2 K	80 K	4.2 K
$[Fe(salen)]_2O^+PF_6^-$	0.427 (5)	0.418 (1)	1.627 (5)	1.540 (1)	0.268 (6), 0.285 (5)	0.237 (2), 0.217 (1)
$[Fe(salen)]_2O^+ClO_4^-$	0.393 (4)	0.410 (3)	1.229 (4)	1.238 (4)	0.269 (4), 0.286 (5)	0.198 (3), 0.208 (3)
$[Fe(salen)]_2O^+BF_4^-$	0.413 (2)		1.535 (2)		0.168 (2), 0.175 (2)	
$[Fe(salen)]_2O^+I_3^-\cdot CHCl_3$	0.389 (1)	0.409 (3)	1.310 (1)	1.283 (3)	0.145 (1), 0.143 (1)	0.235 (3), 0.213 (3)
$(FeTPP)_2O^+PF_6^-$	0.332 (1)	0.348 (4)	1.272 (1)	1.244 (4)	0.184 (1), 0.189 (1)	0.246 (5), 0.236 (5)
$(FeTPP)_2O^+BF_4^-$	0.320 (2)		1.411 (2)		0.239 (2), 0.255 (2)	

[a] Relative to Fe metal. [b] Error in last significant figure in parentheses. [c] Half-width at half-maximum listed in the order of increasing velocity of the peak.

Table IV[a]

Compd	X band			Q band	
	300 K	77 K	4.2 K	300 K	77 K
$[Fe(salen)]_2O^+PF_6^-$	1.99 (1160)	1.99 (1220)	1.98 (650)	2.00[b]	2.00[b]
$[Fe(salen)]_2O^+ClO_4^-$	2.01 (360)	2.01[b] (410)	4.31 (140)	2.00 (505)	2.00 (508)
$[Fe(salen)]_2O^+BF_4^-$	2.01 (840)	1.93 (1550)	NS	2.00 (780)	2.00 (2450)
$[Fe(salen)]_2O^+I_3^-\cdot CHCl_3$	1.97[b]	2.02 (1520)	NS	2.00 (1375)	2.00 (1480)[b]
$(FeTPP)_2O^+PF_6^-$	NS	1.95	2.02[b]		
		2.05			
		5.46	5.48		
$(FeTPP)_2O^+BF_4^-$	NS	NS	NS	NS	NS

[a] Line widths (hwhm) are given in parentheses in units of gauss; NS = no signal. [b] Unresolved shoulder at low-field side.

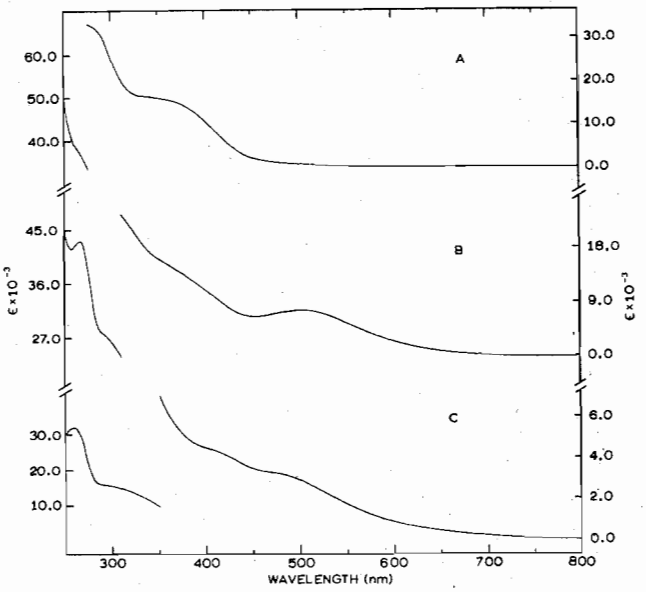

Figure 4. CH_2Cl_2 solution electronic absorption spectra of (A) $[Fe(salen)]_2O$, (B) $[Fe_2(salen)_2O]I_3\cdot CHCl_3$, and (C) $[Fe_2(salen)_2O]PF_6$ at room temperature. The molar extinction coefficients, ϵ, are in units of M^{-1} cm^{-1}. The left-hand ordinates are for the short-wavelength curves, while the right-hand ordinates are for the long-wavelength curves.

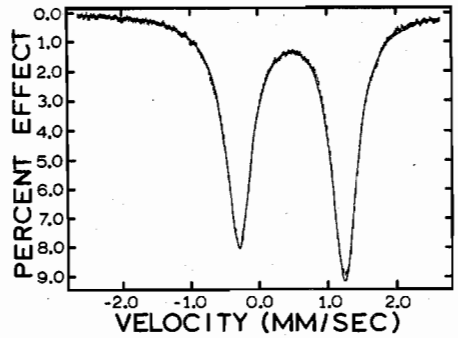

Figure 5. The 4.2-K ^{57}Fe Mössbauer spectrum of $[Fe_2(salen)_2O]PF_6$. The velocity scale is referenced to iron metal.

$en)_2O]X$ compounds. Weak ligand vibrations do occur at 890 and 865 cm^{-1}, as well as strong ligand vibrations at 910 and 800 cm^{-1}.

Mixed-valence compounds characteristically show intervalence-transfer bands in their electronic absorption spectra.[31,32] The solution electronic absorption spectrum of $[Fe(salen)]_2O$ is featureless throughout the visible region of the spectrum and has a broad absorption at 350 nm,[33] as shown in Figure 4. This broad band is shifted to higher energy ($\sim$300 nm) and is partially resolved into two absorptions for the $[Fe_2(salen)_2O]X$ compounds. More importantly, broad absorptions appear as unresolved shoulders in the 470-nm region for the $X^- = ClO_4^-$, PF_6^-, and BF_4^- complexes and as a resolved peak at 500 nm for the I_3^- compound. The electronic absorption spectra of $[Fe_2(salen)_2O]PF_6$ and $[Fe_2(salen)_2O]I_3\cdot CHCl_3$ are illustrated in Figure 4. No peaks were observed in the near-IR region of the spectrum.

Iron-57 Mössbauer spectra were run at liquid nitrogen and liquid helium temperatures. In each case, the spectrum consisted of a single quadrupole-split doublet. The 4.2-K spectrum of $[Fe_2(salen)_2O]PF_6$ is shown in Figure 5. Each doublet spectrum was readily least-squares fit with Lorentzian lines; the fitting parameters are summarized in Table III. It can be seen that the isomer shifts are in the range 0.39–0.43 mm/s relative to iron metal and the quadrupole splittings are in the range 1.3–1.6 mm/s. The isomer shifts and quadrupole splittings do not show any unusual temperature dependencies. There is no sign of magnetic broadening in the 4.2-K spectra which is evidence for an exchange interaction that leads to rapid electron spin relaxation that effectively averages the internal magnetic fields to zero. The line widths of the various features are reasonably close to natural line widths. Thus, there is no evidence for two overlapping doublets in any of the spectra.

Room-temperature and near liquid nitrogen temperature EPR spectra were obtained for each of the $[Fe_2(salen)_2O]X$ compounds at both X-band and Q-band frequencies, and near liquid helium temperature spectra were obtained for each compound with the X-band spectrometer. Observables are summarized in Table IV. The liquid nitrogen temperature X-band spectrum of a solid sample of $[Fe_2(salen)_2O]I_3\cdot CHCl_3$ and the liquid helium temperature X-band spectrum of $[Fe_2(salen)_2O]PF_6$ are shown in Figure 6.

At room temperature and at $\sim$77 K, the X-band spectrum of each of the $[Fe_2(salen)_2O]X$ compounds shows a broad signal ($\sim$1000 G hwhm) in the $g = 2$ region. At liquid helium

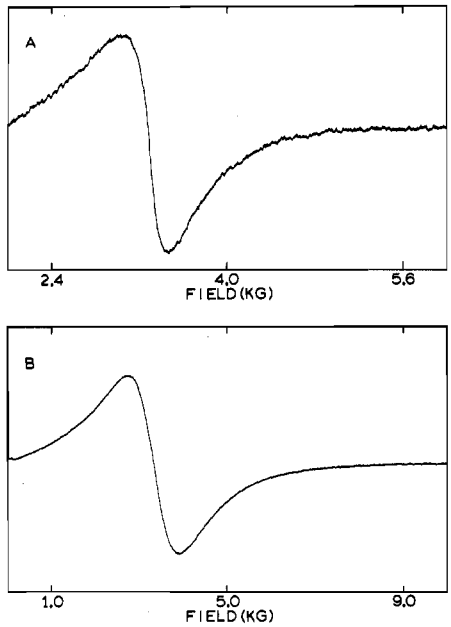

Figure 6. X-Band EPR spectra of solid samples of (A) $[Fe_2(salen)_2O]PF_6$ at near liquid helium temperature and (B) $[Fe_2(salen)_2O]I_3 \cdot CHCl_3$ at near liquid nitrogen temperature.

temperature, *only* $[Fe_2(salen)_2O]PF_6$ still gave a signal at $g \simeq 2$ with a line width of 650 G. At liquid helium temperature, $[Fe_2(salen)_2O]ClO_4$ shows a weak $g = 4.3$ signal, which can be seen, in fact, as a shoulder on the $g \simeq 2$ signal at liquid nitrogen temperature. The $g = 4.3$ signal is probably due to some high-spin ferric impurity as substantiated by the ^{57}Fe Mössbauer spectrum of this compound. In the case of the ClO_4^- compound, the line width of the $g \simeq 2$ signal is 360 G at room temperature and 410 G at liquid nitrogen temperature. The corresponding $g \simeq 2$ signal line widths are 840 and 1550 G, respectively, for the BF_4^- compound. Similarly, the $g \simeq 2$ signal line widths are ~1000 and 1550 G, respectively, for the I_3^- compound. In summary, the X-band EPR signal seen for all the $[Fe_2(salen)_2O]X$ compounds is simply one derivative at $g \simeq 2$ with a temperature-dependent line width.

Similar line width temperature effects are seen in the Q-band EPR spectra. Signals at $g \simeq 2$ are seen for each compound at room and liquid nitrogen temperature. The $g \simeq 2$ signal for $[Fe_2(salen)_2O]ClO_4$ has a temperature-independent line width of ~506 G. At room temperature, the line width for the BF_4^- $g \simeq 2$ signal is 780 G and this is increased to 2450 G by decreasing the temperature to the liquid nitrogen value. The corresponding Q-band line widths for the I_3^- compound are 1375 and 1480 G, respectively.

$[Fe_2(TPP)_2O]X$. The oxidized Fe–TPP compounds are similar to the $[Fe(salen)_2O]X$ compounds in many respects, but there are also differences. The variable-temperature magnetic susceptibilities of $[Fe_2(TPP)_2O]PF_6$ and $[Fe_2(TPP)_2O]BF_4$ indicate the presence of antiferromagnetically coupled dimers. The 267 K effective magnetic moments for these two compounds are 4.17 and 4.26 μ_B, respectively, and as the temperature is decreased to 4.2 K, these values decrease to 1.90 and 1.56 μ_B. Figure 7 illustrates the data obtained for $[Fe_2(TPP)_2O]BF_4$. Attempts to fit the data for each of the two compounds to the perturbation theory equations[22,23] for isotropic exchange in either an $S_1 = {}^5/_2$, $S_2 = 2$ dimer or an $S_1 = {}^3/_2$, $S_2 = 2$ dimer or even an $S_1 = S_2 = {}^5/_2$ dimer failed to give satisfactory fits. Iron(III) porphyrins are known to possess large, axial, single-ion, zero-field splittings (i.e., $D\hat{S}_Z^2$). For example, far-infrared measurements[34] on certain high-spin ferric porphyrins found zero-field splitting D values in the range of 5–17 cm^{-1}. Thus, it was thought that inclusion of an axial zero-field splitting term in the spin Hamiltonian for

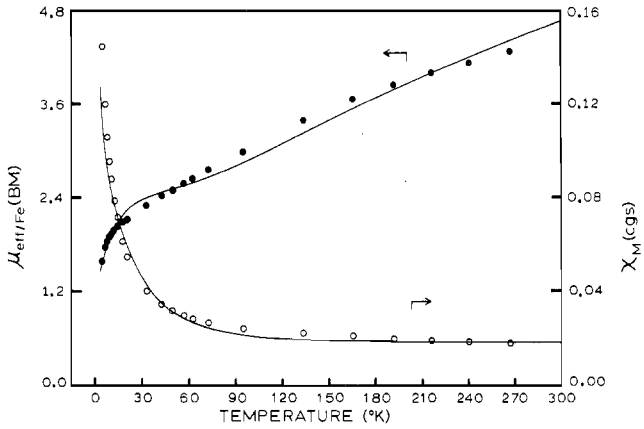

Figure 7. Molar paramagnetic susceptibility in cgsu and effective magnetic moment per iron in μ_B vs. temperature curves for $[Fe_2(TPP)_2O]BF_4$. The solid lines result from least-squares fitting of the data with the ($S_1 = {}^5/_2$, $S_2 = 2$) isotropic exchange diagonalization procedure (see Appendix), which includes axial zero-field splitting.

an $S_1 = {}^5/_2$, $S_2 = 2$ dimer was needed and justified. It was decided that a perturbation calculation would not suffice, because the parameters J and D may be of comparable magnitude. Thus, as detailed in the Appendix, numerical diagonalization of the Hamiltonian matrix including axial zero-field splitting was selected as the approach to least-squares fit the data. To limit the available parameters, it was necessary to assume that the D values are the same for the Fe(III) and Fe(IV) centers. The procedure followed in fitting the data by direct diagonalization was to initially select $g_\parallel = 2.0$ and $g_\perp = 6.0$ and allow J and D to vary. The resulting values for J and D were then used as initial guesses for a second minimization calculation in which all four parameters, J, D, $g_\parallel$, and $g_\perp$, were allowed to vary. As indicated in Table II, the J values obtained in this way are −119 and −82.5 cm^{-1} for the PF_6^- and BF_4^- compounds, respectively. The corresponding zero-field splitting parameters are 11.7 and 19.9 cm^{-1}, respectively. As seems reasonable, the sign of D *cannot* be determined in this fitting, because it was found that either a positive or negative D value of the same magnitude gave a similar fit. From the fitting, it was found that $g_\parallel = 2.34$ and $g_\perp = 5.47$ for $[Fe_2(TPP)_2O]PF_6$. These values are amazingly close to the experimental g values (vide infra). For the BF_4^- compound, the fitting gave $g_\parallel = 3.11$ and $g_\perp = 4.80$. The least-squares fit for this compound is represented in Figure 7 as solid lines and observed and calculated values of χ_M and μ_{eff} are listed in Table V. In passing, it should be mentioned that least-squares fits obtained with procedures other than that described were tried, but inferior fits were obtained.

The infrared spectra of the $[Fe_2(TPP)_2O]X$ compounds, after a fashion, resemble those of the $[Fe_2(salen)_2O]X$ compounds. That is, the 870- and 890-cm^{-1} absorptions which have been assigned[35] to the asymmetric Fe–O–Fe stretch are absent in the oxidized compounds. Again, the intensities of the ligand vibrational modes are about the same in the unoxidized and oxidized dimers. In addition, some of the ligand vibrations increase in energy by 10–20 cm^{-1}. The 30-K, KBr-pellet spectra of $[Fe(TPP)]_2O$ and $[Fe_2(TPP)_2O]BF_4$ are shown in Figure 8. The numerous ligand vibrations make it very difficult to tell if the Fe–O–Fe band has shifted close to some ligand band. In fact, attention is drawn to the apparent broadening of the band at 798 cm^{-1}. A recent investigation of the symmetric and asymmetric Fe–O–Fe stretching vibrations indicated that a 50–70-cm^{-1} decrease of the frequencies may occur for an angular Fe–O–Fe species relative to a more linear Fe–O–Fe.[36] It is possible, then, that the Fe–O–Fe unit is more angular in the oxidized compounds.

Table V. Magnetic Susceptibility Data for $[Fe_2(TPP)_2O]BF_4$[a]

	$10^3\chi_M$, cgsu		μ_{eff}/Fe, μ_B	
T, K	Obsd	Calcd	Obsd	Calcd
267	16.99	18.34	4.26	4.42
240	17.53	18.41	4.11	4.21
216	18.30	18.51	3.98	4.00
192	19.05	18.66	3.82	3.78
166	20.02	18.90	3.64	3.54
134	21.27	19.44	3.37	3.22
94.9	23.10	21.29	2.96	2.84
72.5	25.75	24.36	2.73	2.66
62.4	27.50	26.88	2.62	2.59
56.9	28.72	28.73	2.56	2.56
50.0	30.68	31.69	2.48	2.52
42.7	33.81	35.84	2.40	2.47
33.0	39.41	43.73	2.28	2.40
20.6	53.57	60.57	2.10	2.23
17.7	60.38	66.23	2.07	2.17
14.3	70.70	74.06	2.01	2.06
12.3	77.65	79.46	1.95	1.98
10.5	86.74	85.10	1.91	1.89
9.4	94.50	89.12	1.89	1.83
7.9	104.6	95.73	1.82	1.74
6.4	118.7	104.7	1.74	1.64
4.2	144.0	127.4	1.56	1.46

[a] The diamagnetic correction used is -638×10^{-6} cgsu/mol.

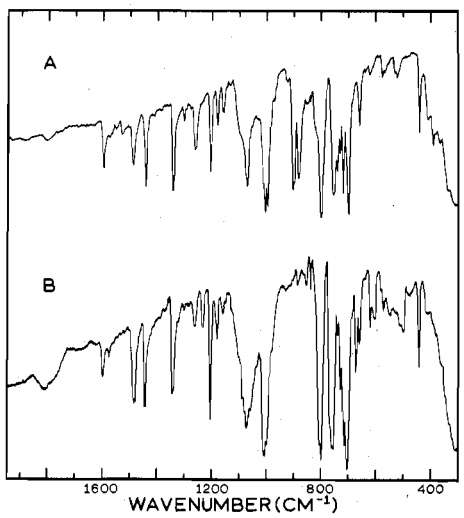

Figure 8. The 30-K IR spectra of (A) $[Fe(TPP)]_2O$ and (B) $[Fe_2(TPP)_2O]BF_4$, run as KBr pellets.

This would cause a 50–70-cm^{-1} decrease in the Fe–O–Fe stretching frequency, which would lead to an overlap with a ligand band.

The ^{57}Fe Mössbauer spectra for $[Fe_2(TPP)_2O]PF_6$ and $[Fe_2(TPP)_2O]BF_4$ are similar to those of the salen compounds in that a single quadrupole-split doublet is observed in each spectrum. The 4.2-K spectrum of $[Fe_2(TPP)_2O]PF_6$ is shown in Figure 9. Again, there is no unusual temperature dependence in either the isomer shifts or quadrupole splittings (see Table III). At liquid nitrogen temperatures, isomer shifts of 0.32–0.33 mm/s (relative to iron metal) and quadrupole splittings of 1.27–1.41 mm/s are seen for the $[Fe_2(TPP)_2O]X$ compounds. The isomer shifts observed for oxo-bridged iron(III) porphyrins[37] and monomeric iron(III) porphyrins[38] are in the range of 0.40–0.46 mm/s. The more negative isomer shift values observed for the $[Fe_2(TPP)_2O]X$ compounds are indicative of a more highly oxidized state of iron. For ^{57}Fe a higher oxidation state leads to a greater s-electron density at the nucleus and since the excited-state nuclear radius is smaller than the ground-state nuclear radius, a more negative isomer shift results. Typical quadrupole splittings for oxo-bridged iron(III) porphyrins and monomeric iron(III) porphyrins are all less than 1.0 mm/s and fall in the range of 0.54–0.73 mm/s. The larger values of quadrupole splittings in the $[Fe_2(TPP)_2O]X$ compounds may be indicative of either a lower symmetry caused by a more angular Fe–O–Fe unit and/or the average higher iron ion oxidation state.

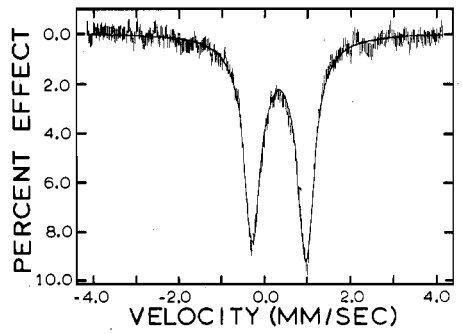

Figure 9. The 4.2-K ^{57}Fe Mössbauer spectrum of $[Fe_2(TPP)_2O]PF_6$. The velocity scale is referenced to iron metal.

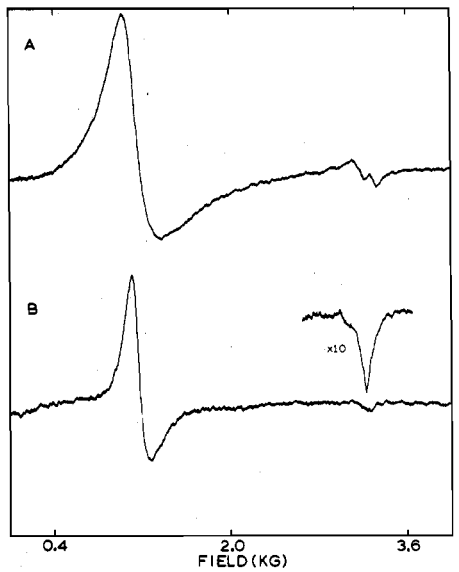

Figure 10. X-Band EPR spectra of a solid sample of $[Fe_2(TPP)_2O]PF_6$ at near liquid nitrogen temperature (A) and at near liquid helium temperature (B).

No EPR signals could be observed for $[Fe_2(TPP)_2O]BF_4$ with either X-band or Q-band frequencies or at any of the temperatures available to us. The PF_6^- compound also did not show a room-temperature signal and the signals seen at low temperatures are quite different from those of the $[Fe_2(salen)_2O]X$ compounds. For example, at liquid nitrogen temperature $[Fe_2(TPP)_2O]PF_6$ gives an X-band spectrum with three features at g values of 5.46, 2.05, and 1.95; see Figure 10. The liquid helium X-band spectrum is very similar. This type of spectrum is typical of high-spin ferric porphyrins.[39]

Solution electronic absorption spectra were obtained for $[Fe_2(TPP)_2O]PF_6$ and $[Fe_2(TPP)_2O]BF_4$. No absorptions were observed in the near-infrared region for either compound. The UV and visible spectra for these two compounds are shown in Figure 11, and for comparison purposes, the spectra of $[Fe(TPP)]_2O$ and Fe(TPP)Cl are shown in Figure 12. It is readily apparent that the spectrum of $[Fe_2(TPP)_2O]PF_6$ is quite similar to that of Fe(TPP)Cl. However, the spectrum of $[Fe_2(TPP)_2O]BF_4$ is certainly *not* identical with those for either $[Fe(TPP)]_2O$ or Fe(TPP)Cl. A comparison of the spectrum of $[Fe_2(TPP)_2O]BF_4$ with that reported[11] for $[Fe_2(TPP)_2O]ClO_4$ shows them to be identical.

Discussion

In regard to the $[Fe_2(salen)_2O]X$ and $[Fe_2(TPP)_2O]X$

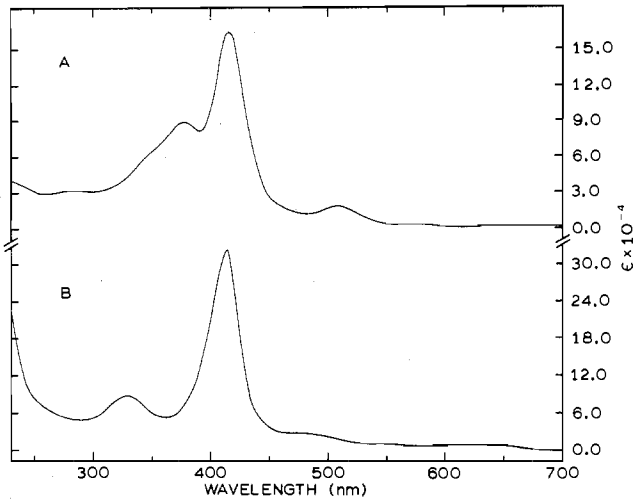

Figure 11. CH_2Cl_2 solution electronic absorption spectra of (A) $[Fe_2(TPP)_2O]PF_6$ and (B) $[Fe_2(TPP)_2O]BF_4$ at room temperature. The molar extinction coefficients, ϵ, are in units of M^{-1} cm^{-1}.

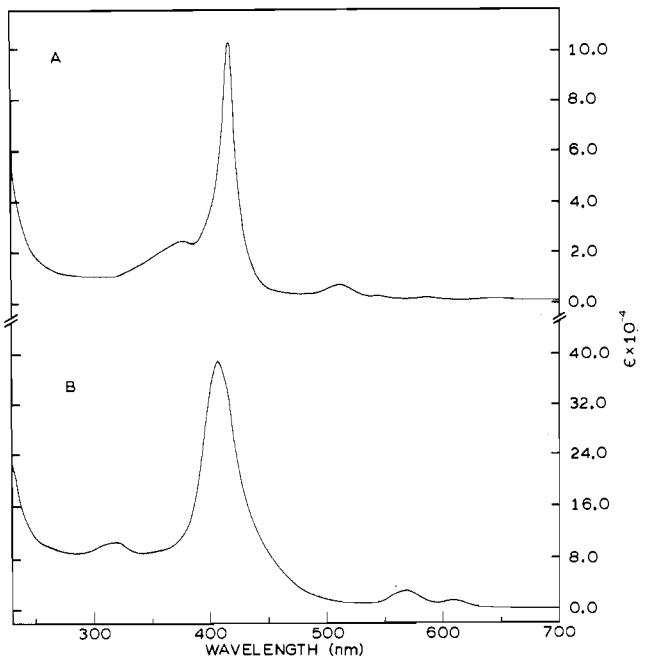

Figure 12. CH_2Cl_2 solution electronic absorption spectra of (A) Fe(TPP)Cl and (B) $[Fe(TPP)]_2O$ at room temperature. The molar extinction coefficients, ϵ, are in units of M^{-1} cm^{-1}.

compounds, there are two points of discussion. First, we need to consider whether the cations in these salts are, in fact, oxo bridged. Second, if these compounds are indeed mixed-valence $Fe^{III}Fe^{IV}$ species, it is important to determine what the thermal electron-transfer rates are.

The assignment of the $[Fe_2(salen)_2O]X$ and $[Fe_2(TPP)_2O]X$ compounds as $Fe^{III}Fe^{IV}$ (i.e., $S_1 = {}^5/_2$, $S_2 = 2$) species is only one of the several possibilities that were considered in the analysis of the data. Unfortunately, crystals suitable for an x-ray structure determination could not be grown, in part because of the solution instability of these oxidized compounds over extended periods. The $S_1 = {}^5/_2$, $S_2 = 2$ characterization is consistent with all of our data. From the magnetic susceptibility data (antiferromagnetic exchange interactions), it is known that there are dimers in the solid. The conductivity of $[Fe_2(salen)_2O]ClO_4$ in ethanol clearly points to a 1:1 electrolyte. The apparent absence of an asymmetric Fe–O–Fe stretching band in the infrared spectrum leads one to consider whether the bridging is other than μ-oxo.

It is possible to formulate the dimeric cations as di-μ-hydroxo-bridged $Fe^{III}Fe^{IV}$ species, e.g., $[Fe_2(salen)_2(OH)_2]PF_6$. The relatively small magnetic-exchange J values (−17.6 to −7.5 cm^{-1}) could support this, for it has been reported[40] that the di-μ-hydroxo compound $[Fe(pic)_2(OH)]_2$ gives susceptibility data which fit to the equations for an isotropic exchange interaction in a Fe(III) dimer, $S_1 = S_2 = {}^5/_2$, and give $J = -8$ cm^{-1}. A broad and weak absorption at 900–1000 cm^{-1} has been assigned to the bridging OH deformation mode.[8,40] We prepared a sample of $[Fe(pic)_2(OH)]_2$, as the diaquo adduct, and ran the IR spectrum of this compound (KBr pellet) at room temperature and 30 K. The 950-cm^{-1} peak, which has been assigned to the $Fe_2(OH)_2^{4+}$ unit, exhibits a distinctive temperature dependence. At room temperature, the absorption at 948 cm^{-1} is broad and of medium intensity relative to the other peaks in the spectrum. At 30 K, the peak shifts to 960 cm^{-1}, becomes less broad, and increases in relative intensity by a factor of about 2. This type of behavior is *not* seen for any of the 800–1100-cm^{-1} peaks in the $[Fe_2(salen)_2O]X$ and $[Fe_2(TPP)_2O]X$ IR spectra. We believe that we do *not* have di-μ-hydroxo bridging.

Another type of bridging possibility is that found in $[Fe(salen)Cl]_2$.[41] In this compound a dimer is formed by two square-pyramidal units where the two basal planes are parallel and are in close proximity. An oxygen atom of the salen bonded to one Fe(III) ion also bonds to the second Fe(III) ion. The bridging unit is

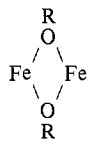

The compound $[Fe(salen)Cl]_2$ does show an antiferromagnetic-exchange interaction[42] between the two Fe(III) ions ($S_1 = S_2 = {}^5/_2$) with $J \simeq -7.5$ cm^{-1}. If the compounds that we made have this type of bridging structure, the dimeric association in the cation would have to be between a five-coordinate hydroxo–ferric unit and perhaps a five-coordinate aquo–ferric unit, e.g., $[Fe_2(salen)_2(OH)(H_2O)]PF_6$. At this time, we do not believe that this type of dimeric association is present because this dimer would be expected to dissociate readily in solution and we have found that $[Fe(salen)_2O]ClO_4$ is a 1:1 electrolyte in ethanol. It should also be added that $[Fe(salen)Cl]_2$ has an IR band at 850 cm^{-1} which has been attributed to the

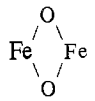

unit.[43] Furthermore, there would be sizable steric interactions which would make such a dimeric association very unfavorable in the TPP compounds.

Two other bridging possibilities should be mentioned briefly. Neither has much precedence in iron chemistry. A mono-μ-hydroxo bridge, which requires two Fe(III) ions with $S_1 = S_2 = {}^5/_2$, is a possibility, e.g., $[Fe_2(salen)_2(OH)]PF_6$. Such a formulation is not consistent with the best fit to the observed susceptibility data. Another possibility is a peroxide (O_2^{2-}) bridge. For our compounds, this would formally require a $Fe^{III}Fe^{IV}$ species. Very recently a dioxygen-bridged iron(II) compound was reported.[44] Without giving much detail, this compound was identified as a Fe(II) dimer bridged by singlet dioxygen.

Thus, we are not absolutely sure that the $[Fe_2(salen)_2O]X$ and $[Fe_2(TPP)_2O]X$ compounds do have μ-oxo bridging. We are continuing our efforts to secure good crystals of one of the compounds, but work to date has shown that this will not be easy. Irrespective of the details of the bridging mode that is

present, it seems clear that there are mixed-valence $Fe^{III}Fe^{IV}$ dimers present in the solids.

Two types of ^{57}Fe Mössbauer spectra would be expected for an exchange-interacting, binuclear iron complex in which the iron ions are formally in different oxidation states. The presence of an exchange interaction will permit a thermal electron transfer between the two iron ions. The "extra" electron associated with the Fe(III) ion will transfer to the Fe(IV) ion, thereby reversing the oxidation labels. If the thermal rate of electron transfer is slower than the ^{57}Fe Mössbauer time scale ($\sim 10^7$ s^{-1}), two quadrupole-split doublets will be seen in the spectrum, one for the Fe(III) center and the other for the Fe(IV) center. If, on the other hand, the rate is somewhat faster than $\sim 10^7$ s^{-1}, the spectrum will consist of only one doublet. The dimeric complex will be average valence on the ^{57}Fe Mössbauer time scale. All of the $[Fe_2(salen)_2O]X$ and $[Fe(TPP)_2O]X$ compounds exhibited only one doublet, and, as such, it can be concluded that the thermal electron-transfer rate is greater than $\sim 10^7$ s^{-1}. The likelihood of an overlapping pair of doublets arising from two different iron centers is minimal, because the observed line widths are reasonably close to natural line widths.

For an $S_1 = {}^5/_2$, $S_2 = 2$, $Fe^{III}Fe^{IV}$ binuclear complex, an EPR spectrum consisting of the superposition of high-spin Fe(III) and high-spin Fe(IV) signals would be expected if the rate of thermal electron transfer is slower than the EPR time scale ($\sim 10^{10}$ s^{-1}). A high-spin Fe(IV) complex would probably have EPR characteristics similar to those of a high-spin Fe(II) complex. High-spin Fe(II) complexes are notorious for very rapid spin–lattice relaxation times and, as a result, EPR signals are very difficult to detect. Thus, for electron-transfer rates less than $\sim 10^{10}$ s^{-1}, the EPR spectrum of a $Fe^{III}Fe^{IV}$ would be similar to the spectrum of a high-spin Fe(III) complex. This is the type of spectrum that we obtained for $[Fe_2(TPP)_2O]PF_6$ and we conclude that the thermal electron-transfer rate for this compound is less than $\sim 10^{10}$ s^{-1}.

For rates greater than $\sim 10^{10}$ s^{-1}, the EPR spectrum of the formally $Fe^{III}Fe^{IV}$ species will exhibit a relatively isotropic signal. In our work[10] on mixed-valence fused ferrocenes, we found that in going from a species with a slow transfer rate to a species with a rate greater than $\sim 10^{10}$ s^{-1} the **g** tensor changed from anisotropic to relatively isotropic. With the greater rates of transfer, the EPR signal is exchange averaged. Furthermore, if the rate of electron transfer is close to that which would give complete averaging, then an EPR spectrum would be seen that exhibits a pronounced temperature-dependent line width. The EPR spectra of the $[Fe_2(salen)_2O]X$ compounds show a single $g \simeq 2.0$ derivative which is somewhat temperature dependent in line width. Thus, the rate of thermal electron transfer in these compounds is on the order of $\sim 10^{10}$ s^{-1}.

A comparison of the EPR data reported[11] for oxidized oxo-bridged iron porphyrins with the EPR data for our two $[Fe_2(TPP)_2O]X$ compounds shows some differences. At liquid nitrogen temperatures, a solid sample of $[Fe_2(TPP)_2O]ClO_4$ was reported[11] to give *very weak* signals at $g = 2.059$ and 1.993. Our EPR data are *not* necessarily in disagreement with these results. Unfortunately, we have been unable to prepare a good sample of $[Fe_2(TPP)_2O]ClO_4$ by a chemical oxidation. We did not see an EPR signal for $[Fe_2(TPP)_2O]BF_4$ and this could be the consequence of having an even weaker signal (or perhaps lower instrumental signal-to-noise ratio) than was observed for the ClO_4^- salt. A change in the anion would be expected to affect the structure of the cation; a structural change (e.g., Fe–O–Fe angle) in the cation could change the *intra*dimer thermal electron-transfer rate. A slight change of this rate would probably affect the EPR signal very dramatically, particularly if the rate is close to the microwave frequency.

An explanation for the relatively slow thermal electron transfer in these oxo-bridged $Fe^{III}Fe^{IV}$ species could be found in differences of the iron ion distance from the plane of the ligand TPP (or salen). If there is an appreciable difference in this distance between the Fe(III) and the Fe(IV) halves of the dimer, then a transfer of an electron from the Fe(III) to the Fe(IV) ion results in a change from the Fe(III)Fe′(IV) ground state to an Fe(IV)Fe′(III) excited state that is at higher energy, and this would lead to a relatively slow thermal electron transfer.

Conclusion

The compounds $[Fe_2(salen)_2O]X$ ($X^- = PF_6^-$, ClO_4^-, BF_4^-, $I_3^-\cdot CHCl_3$) and $[Fe_2(TPP)_2O]X$ ($X^- = PF_6^-$ and BF_4^-) have been shown to be composed of dimeric cations that are mixed valence, $Fe^{III}Fe^{IV}$. Variable-temperature IR measurements have not located asymmetric Fe–O–Fe stretching bands and, as such, the precise bridging nature of the dimeric cation is not known. Mössbauer and EPR experiments have shown that the thermal electron-transfer rates are on the order of $\sim 10^{10}$ s^{-1}.

Acknowledgment. We thank Professor P. G. Debrunner and Mr. C. R. Hill for assistance with the ^{57}Fe Mössbauer work. We are grateful for partial funding of this research by National Institutes of Health Grant HL 13652.

Appendix

The spin Hamiltonian which describes an isotropic exchange coupled pair of iron ions including axial zero-field splitting on centers 1 and 2 is

$$\hat{H} = -2J\hat{S}_1\cdot\hat{S}_2 + D_1(\hat{S}_{Z1}^2 - {}^1/_3\hat{S}_1^2) + D_2(\hat{S}_{Z2}^2 - {}^1/_3\hat{S}_2^2) + g_1\beta\hat{H}\cdot\hat{S}_1 + g_2\beta\hat{H}\cdot\hat{S}_2$$

In this equation, J is the exchange parameter, D_1 and D_2 are the axial zero-field splitting parameters for centers 1 and 2, respectively, $\hat{S}_1$ and $\hat{S}_2$ are the spin operators for centers 1 and 2, respectively, $\hat{S}_{Z1}$ and $\hat{S}_{Z2}$ are the spin operator projections on the axis of quantization for centers 1 and 2, respectively, $\hat{H}$ is the magnetic field, g_1 and g_2 are the electronic g values for centers 1 and 2, respectively, and β is the Bohr magneton. The basis set selected is the coupled spin basis set defined by

$$|S_1S_2S'M'_S\rangle = (-1)^{S_2-S_1-M'_S}\sum_{M_{S1},M_{S2}}(2S'+1)^{1/2}\begin{pmatrix} S_1 & S_2 & S' \\ M_{S1} & M_{S2} & M'_S \end{pmatrix}|S_1S_2M_{S1}M_{S2}\rangle$$

In this equation, $S' \equiv S_1 + S_2$, $M'_S = M_{S1} + M_{S2}$, and

$$\begin{pmatrix} S_1 & S_2 & S' \\ M_{S1} & M_{S2} & M'_S \end{pmatrix}$$

is the $3-j$ symbol representation of the Wigner coefficient.

When the simplifying assumptions $D \equiv D_1 = D_2$ and $g \equiv g_1 = g_2$ are made, the above Hamiltonian operator becomes

$$\hat{H} = -J\hat{S}'^2 + D[\hat{S}_{Z1}^2 + \hat{S}_{Z2}^2] + g\beta\hat{H}\cdot\hat{S}' = \hat{H}_{J,D} + \hat{H}_M$$

The spin operators $D_1\hat{S}_1^2$, $D_2\hat{S}_2^2$, $-J\hat{S}_1^2$, and $-J\hat{S}_2^2$ have been dropped since they contribute a constant energy to each energy level. When $S_1 = {}^5/_2$ and $S_2 = 2$, a 30×30 Hamiltonian matrix is obtained. Operating on the coupled spin basis set with the above Hamiltonian excluding the Zeeman interaction yields the diagonal matrix elements given below. For simplicity, we take $|S_1S_2S'M'_S\rangle \equiv |S'M'_S\rangle$.

$\langle {}^9/_2 \pm {}^9/_2|\hat{H}_{J,D}|{}^9/_2 \pm {}^9/_2\rangle = -99J/4 + 41D/4$
$\langle {}^9/_2 \pm {}^7/_2|\hat{H}_{J,D}|{}^9/_2 \pm {}^7/_2\rangle = -99J/4 + 241D/36$
$\langle {}^9/_2 \pm {}^5/_2|\hat{H}_{J,D}|{}^9/_2 \pm {}^5/_2\rangle = -99J/4 + 145D/36$
$\langle {}^9/_2 \pm {}^3/_2|\hat{H}_{J,D}|{}^9/_2 \pm {}^3/_2\rangle = -99J/4 + 189D/84$
$\langle {}^9/_2 \pm {}^1/_2|\hat{H}_{J,D}|{}^9/_2 \pm {}^1/_2\rangle = -99J/4 + 323D/252$
$\langle {}^7/_2 \pm {}^7/_2|\hat{H}_{J,D}|{}^7/_2 \pm {}^7/_2\rangle = -63J/4 + 245D/36$
$\langle {}^7/_2 \pm {}^5/_2|\hat{H}_{J,D}|{}^7/_2 \pm {}^5/_2\rangle = -63J/4 + 1307D/252$
$\langle {}^7/_2 \pm {}^3/_2|\hat{H}_{J,D}|{}^7/_2 \pm {}^3/_2\rangle = -63J/4 + 345D/84$
$\langle {}^7/_2 \pm {}^1/_2|\hat{H}_{J,D}|{}^7/_2 \pm {}^1/_2\rangle = -63J/4 + 899D/252$
$\langle {}^5/_2 \pm {}^5/_2|\hat{H}_{J,D}|{}^5/_2 \pm {}^5/_2\rangle = -35J/4 + 127D/28$
$\langle {}^5/_2 \pm {}^3/_2|\hat{H}_{J,D}|{}^5/_2 \pm {}^3/_2\rangle = -35J/4 + 699D/140$
$\langle {}^5/_2 \pm {}^1/_2|\hat{H}_{J,D}|{}^5/_2 \pm {}^1/_2\rangle = -35J/4 + 731D/140$
$\langle {}^3/_2 \pm {}^3/_2|\hat{H}_{J,D}|{}^3/_2 \pm {}^3/_2\rangle = -15J/4 + 511D/140$
$\langle {}^3/_2 \pm {}^1/_2|\hat{H}_{J,D}|{}^3/_2 \pm {}^1/_2\rangle = -15J/4 + 2597D/420$
$\langle {}^1/_2 \pm {}^1/_2|\hat{H}_{J,D}|{}^1/_2 \pm {}^1/_2\rangle = -3J/4 + 59D/12$

The nondiagonal matrix elements of the lower triangle of the Hamiltonian matrix are

$\langle {}^7/_2 + {}^7/_2|\hat{H}_{J,D}|{}^9/_2 + {}^7/_2\rangle = 2(5^{1/2})D/9$
$= -\langle {}^9/_2 - {}^7/_2|\hat{H}_{J,D}|{}^7/_2 - {}^7/_2\rangle$
$\langle {}^7/_2 + {}^5/_2|\hat{H}_{J,D}|{}^9/_2 + {}^5/_2\rangle = 5(35^{1/2})D/63$
$= -\langle {}^9/_2 - {}^5/_2|\hat{H}_{J,D}|{}^7/_2 - {}^5/_2\rangle$
$\langle {}^5/_2 + {}^5/_2|\hat{H}_{J,D}|{}^9/_2 + {}^5/_2\rangle = 2(105^{1/2})D/21$
$= \langle {}^9/_2 - {}^5/_2|\hat{H}_{J,D}|{}^5/_2 - {}^5/_2\rangle$
$\langle {}^7/_2 + {}^3/_2|\hat{H}_{J,D}|{}^9/_2 + {}^3/_2\rangle = 5^{1/2}D/7$
$= -\langle {}^9/_2 - {}^3/_2|\hat{H}_{J,D}|{}^7/_2 - {}^3/_2\rangle$
$\langle {}^5/_2 + {}^3/_2|\hat{H}_{J,D}|{}^9/_2 + {}^3/_2\rangle = 10D/7$
$= \langle {}^9/_2 - {}^3/_2|\hat{H}_{J,D}|{}^5/_2 - {}^3/_2\rangle$
$\langle {}^3/_2 + {}^3/_2|\hat{H}_{J,D}|{}^9/_2 + {}^3/_2\rangle = -6^{1/2}D/21$
$= -\langle {}^9/_2 - {}^3/_2|\hat{H}_{J,D}|{}^3/_2 - {}^3/_2\rangle$
$\langle {}^7/_2 + {}^1/_2|\hat{H}_{J,D}|{}^9/_2 + {}^1/_2\rangle = 5(2^{1/2})D/63$
$= -\langle {}^9/_2 - {}^1/_2|\hat{H}_{J,D}|{}^7/_2 - {}^1/_2\rangle$
$\langle {}^5/_2 + {}^1/_2|\hat{H}_{J,D}|{}^9/_2 + {}^1/_2\rangle = 20(3^{1/2})D/21$
$= \langle {}^9/_2 - {}^1/_2|\hat{H}_{J,D}|{}^5/_2 - {}^1/_2\rangle$
$\langle {}^3/_2 + {}^1/_2|\hat{H}_{J,D}|{}^9/_2 + {}^1/_2\rangle = 0 = \langle {}^1/_2 + {}^1/_2|\hat{H}_{J,D}|{}^9/_2 + {}^1/_2\rangle$
$= \langle {}^9/_2 - {}^1/_2|\hat{H}_{J,D}|{}^3/_2 - {}^1/_2\rangle = \langle {}^9/_2 - {}^1/_2|\hat{H}_{J,D}|{}^1/_2 - {}^1/_2\rangle$
$\langle {}^5/_2 + {}^5/_2|\hat{H}_{J,D}|{}^7/_2 + {}^5/_2\rangle = 11(3^{1/2})D/21$
$= -\langle {}^7/_2 - {}^5/_2|\hat{H}_{J,D}|{}^5/_2 - {}^5/_2\rangle$
$\langle {}^5/_2 + {}^3/_2|\hat{H}_{J,D}|{}^7/_2 + {}^3/_2\rangle = 11(5^{1/2})D/35$
$= -\langle {}^7/_2 - {}^3/_2|\hat{H}_{J,D}|{}^5/_2 - {}^3/_2\rangle$
$\langle {}^3/_2 + {}^3/_2|\hat{H}_{J,D}|{}^7/_2 + {}^3/_2\rangle = 36(30^{1/2})D/105$
$= \langle {}^7/_2 - {}^3/_2|\hat{H}_{J,D}|{}^3/_2 - {}^3/_2\rangle$
$\langle {}^5/_2 + {}^1/_2|\hat{H}_{J,D}|{}^7/_2 + {}^1/_2\rangle = 11(6^{1/2})D/105$
$= -\langle {}^7/_2 - {}^1/_2|\hat{H}_{J,D}|{}^5/_2 - {}^1/_2\rangle$
$\langle {}^3/_2 + {}^1/_2|\hat{H}_{J,D}|{}^7/_2 + {}^1/_2\rangle = 36(6^{1/2})D/35$
$= \langle {}^7/_2 - {}^1/_2|\hat{H}_{J,D}|{}^3/_2 - {}^1/_2\rangle$
$\langle {}^1/_2 + {}^1/_2|\hat{H}_{J,D}|{}^7/_2 + {}^1/_2\rangle = 0 = \langle {}^7/_2 - {}^1/_2|\hat{H}_{J,D}|{}^1/_2 - {}^1/_2\rangle$
$\langle {}^3/_2 + {}^3/_2|\hat{H}_{J,D}|{}^5/_2 + {}^3/_2\rangle = 22(6^{1/2})D/35$
$= -\langle {}^5/_2 - {}^3/_2|\hat{H}_{J,D}|{}^3/_2 - {}^3/_2\rangle$
$\langle {}^3/_2 + {}^1/_2|\hat{H}_{J,D}|{}^5/_2 + {}^1/_2\rangle = 22D/35$
$= -\langle {}^5/_2 - {}^1/_2|\hat{H}_{J,D}|{}^3/_2 - {}^1/_2\rangle$
$\langle {}^1/_2 + {}^1/_2|\hat{H}_{J,D}|{}^5/_2 + {}^1/_2\rangle = 28(14^{1/2})D/35$
$= \langle {}^5/_2 - {}^1/_2|\hat{H}_{J,D}|{}^1/_2 - {}^1/_2\rangle$
$\langle {}^1/_2 + {}^1/_2|\hat{H}_{J,D}|{}^3/_2 + {}^1/_2\rangle = 77(14^{1/2})D/105$
$= -\langle {}^3/_2 - {}^1/_2|\hat{H}_{J,D}|{}^1/_2 - {}^1/_2\rangle$

When the magnetic field is parallel to the z axis of the molecule, the Hamiltonian which describes the Zeeman interaction becomes $\hat{H}_M = g_\parallel \beta \hat{H}\cdot\hat{S}'$.[1] The resulting Zeeman Hamiltonian matrix is diagonal and the elements of the matrix are

$\langle S' \pm {}^9/_2|\hat{H}_M|S' \pm {}^9/_2\rangle = \pm {}^9/_2 g_\parallel \beta H$
$\langle S' \pm {}^7/_2|\hat{H}_M|S' \pm {}^7/_2\rangle = \pm {}^7/_2 g_\parallel \beta H$
$\langle S' \pm {}^5/_2|\hat{H}_M|S' \pm {}^5/_2\rangle = \pm {}^5/_2 g_\parallel \beta H$
$\langle S' \pm {}^3/_2|\hat{H}_M|S' \pm {}^3/_2\rangle = \pm {}^3/_2 g_\parallel \beta H$
$\langle S' \pm {}^1/_2|\hat{H}_M|S' \pm {}^1/_2\rangle = \pm {}^1/_2 g_\parallel \beta H$

When the magnetic field is parallel to the x axis of the molecule, $\hat{H}_M = g_\perp \beta \hat{H}\cdot\hat{S}_{x'} = {}^1/_2 g_\perp \beta \hat{H}\cdot(\hat{S}_{+'} + \hat{S}_{-'})$ where $\hat{S}_{+'}$ and $\hat{S}_{-'}$ are the usual raising and lowering spin operators, respectively. The off-diagonal elements of the lower triangle of the Hamiltonian matrix arising from this Zeeman interaction are

$\langle {}^9/_2 + {}^7/_2|\hat{H}_M|{}^9/_2 + {}^9/_2\rangle = \langle {}^9/_2 - {}^9/_2|\hat{H}_M|{}^9/_2 - {}^7/_2\rangle$
$= 3g_\perp \beta H/2$
$\langle {}^9/_2 + {}^5/_2|\hat{H}_M|{}^9/_2 + {}^7/_2\rangle = \langle {}^9/_2 - {}^7/_2|\hat{H}_M|{}^9/_2 - {}^5/_2\rangle$
$= 2g_\perp \beta H$
$\langle {}^9/_2 + {}^3/_2|\hat{H}_M|{}^9/_2 + {}^5/_2\rangle = \langle {}^9/_2 - {}^5/_2|\hat{H}_M|{}^9/_2 - {}^3/_2\rangle$
$= 21^{1/2} g_\perp \beta H/2$
$\langle {}^9/_2 + {}^1/_2|\hat{H}_M|{}^9/_2 + {}^3/_2\rangle = \langle {}^9/_2 - {}^3/_2|\hat{H}_M|{}^9/_2 - {}^1/_2\rangle$
$= 6^{1/2} g_\perp \beta H$
$\langle {}^7/_2 + {}^5/_2|\hat{H}_M|{}^7/_2 + {}^7/_2\rangle = \langle {}^7/_2 - {}^7/_2|\hat{H}_M|{}^7/_2 - {}^5/_2\rangle$
$= 7^{1/2} g_\perp \beta H/2$
$\langle {}^7/_2 + {}^3/_2|\hat{H}_M|{}^7/_2 + {}^5/_2\rangle = \langle {}^7/_2 - {}^5/_2|\hat{H}_M|{}^7/_2 - {}^3/_2\rangle$
$= 3^{1/2} g_\perp \beta H$
$\langle {}^7/_2 + {}^1/_2|\hat{H}_M|{}^7/_2 + {}^3/_2\rangle = \langle {}^7/_2 - {}^3/_2|\hat{H}_M|{}^7/_2 - {}^1/_2\rangle$
$= 15^{1/2} g_\perp \beta H/2$
$\langle {}^5/_2 + {}^3/_2|\hat{H}_M|{}^5/_2 + {}^5/_2\rangle = \langle {}^5/_2 - {}^5/_2|\hat{H}_M|{}^5/_2 - {}^3/_2\rangle$
$= 5^{1/2} g_\perp \beta H/2$
$\langle {}^5/_2 + {}^1/_2|\hat{H}_M|{}^5/_2 + {}^3/_2\rangle = \langle {}^5/_2 - {}^3/_2|\hat{H}_M|{}^5/_2 - {}^1/_2\rangle$
$= 2^{1/2} g_\perp \beta H$
$\langle {}^3/_2 + {}^1/_2|\hat{H}_M|{}^3/_2 + {}^3/_2\rangle = \langle {}^3/_2 - {}^3/_2|\hat{H}_M|{}^3/_2 - {}^1/_2\rangle$
$= 3^{1/2} g_\perp \beta H/2$
$\langle {}^1/_2 - {}^1/_2|\hat{H}_M|{}^1/_2 + {}^1/_2\rangle = g_\perp \beta H/2$
$\langle {}^3/_2 - {}^1/_2|\hat{H}_M|{}^3/_2 + {}^1/_2\rangle = g_\perp \beta H$
$\langle {}^5/_2 - {}^1/_2|\hat{H}_M|{}^5/_2 + {}^1/_2\rangle = 3g_\perp \beta H/2$
$\langle {}^7/_2 - {}^1/_2|\hat{H}_M|{}^7/_2 + {}^1/_2\rangle = 2g_\perp \beta H$
$\langle {}^9/_2 - {}^1/_2|\hat{H}_M|{}^9/_2 + {}^1/_2\rangle = 5g_\perp \beta H/2$

Since the energy eigenvalues for $H\|x$ axis and $H\|y$ axis are identical ($E = 0$), only the matrix for $H\|x$ axis is dealt with.

The procedure in fitting the magnetic susceptibility data is to diagonalize the Hamiltonian matrices for $H\|z$ axis and $H\|x$ axis numerically on a computer for three magnetic fields which are separated by 100 G. The slopes of the energy levels as a function of the magnetic field strength are determined and these are used to evaluate the magnetic moments. The parallel and perpendicular molar susceptibilities are calculated by

taking the usual Boltzmann weighted average of the magnetic moments as given in the expression

$$\chi_l = \frac{N}{H} \frac{\sum_i (-\partial E_i/\partial H) \exp(-E_i/kT)}{\sum_i \exp(-E_i/kT)}$$

where $l = x$, y, or z, N is Avogadro's number, H is the magnetic field strength, and the summations are over the energy levels E_i. The total molar paramagnetic susceptibility is taken as

$$\chi_M = {}^1/_3(\chi_\parallel + 2\chi_\perp)$$

Registry No. $[Fe(TPP)]_2O$, 12582-61-5; $[Fe(salen)]_2O$, 18601-34-8; $[Fe(salen)]_2O^+PF_6^-$, 61543-16-6; $[Fe(salen)]_2O^+ClO_4^-$, 61543-17-7; $[Fe(salen)]_2O^+BF_4^-$, 61543-18-8; $[Fe(salen)]_2O^+I_3^-$, 61543-19-9; $(FeTPP)_2O^+PF_6^-$, 61491-25-6; $(FeTPP)_2O^+BF_4^-$, 61491-26-7; $[Fe(1,2\text{-}PS)]_2O$, 18601-35-9; Fe(TPP)Cl, 16456-81-8; ^{57}Fe, 14762-69-7.

Supplementary Material Available: Tables VI–XI, susceptibility data for $[Fe_2(salen)_2O]ClO_4$, $[Fe_2(salen)_2O]BF_4$, $[Fe_2(salen)_2O]\text{-}I_3\cdot CHCl_3$, $[Fe_2(TPP)_2O]PF_6$, $[Fe(salen)]_2O$, and $[Fe(1,2\text{-}PS)]_2O$ (6 pages). Ordering information is given on any current masthead page.

References and Notes

(1) Camille and Henry Dreyfus Fellow, 1972–1977; A. P. Sloan Fellow, 1976–1978.
(2) W. S. Caughey, *Adv. Chem. Ser.*, **No. 100**, 248 (1971).
(3) D. V. DerVartanian and J. LeGall, *Biochim. Biophys. Acta*, **346**, 79 (1974).
(4) C. M. Dobson, N. J. Hoyle, C. F. Geraldes, P. E. Wright, R. J. P. Williams, M. Bruschi, and J. LeGall, *Nature (London)*, **249**, 425 (1974).
(5) K. S. Murray, *Coord. Chem. Rev.*, **12**, 1 (1974).
(6) N. Sadasivan, H. I. Eberspaecher, W. H. Fuchsman, and W. S. Caughey, *Biochemistry*, **8**, 534 (1969).
(7) H. J. Schugar, A. T. Hubbard, F. C. Anson, and H. B. Gray, *J. Am. Chem. Soc.*, **91**, 71 (1969); E. B. Fleischer, J. M. Palmer, T. S. Srivastava, and A. Chatterjee, *ibid.*, **93**, 3162 (1971).
(8) J. A. Thich, C. C. Ou, D. Powers, B. Vasiliou, D. Mastropaolo, J. A. Potenza, and H. J. Schugar, *J. Am. Chem. Soc.*, **98**, 1425 (1976).
(9) J. A. Bertrand, J. L. Breece, A. R. Kalyanaraman, G. J. Long, and W. A. Baker, Jr., *J. Am. Chem. Soc.*, **92**, 5233 (1970); J. A. Bertrand, J. L. Breece, and P. G. Eller, *Inorg. Chem.*, **13**, 125 (1974); J. A. Bertrand and P. G. Eller, *ibid.*, **13**, 927 (1974).
(10) W. H. Morrison, Jr., and D. N. Hendrickson, *Inorg. Chem.*, **14**, 2331 (1975).
(11) R. H. Felton, G. S. Owen, D. Dolphin, A. Forman, D. C. Borg, and J. Fajer, *Ann. N.Y. Acad. Sci.*, **206**, 504 (1973).
(12) A. D. Adler, F. R. Longo, J. D. Finarelli, J. Goldmacher, J. Assour, and L. Korsakoff, *J. Org. Chem.*, **32**, 476 (1967).
(13) E. B. Fleischer, J. M. Palmer, T. S. Srivastava, and A. Chatterjee, *J. Am. Chem. Soc.*, **93**, 3162 (1971).
(14) H. Kobayashi and Y. Yanagawa, *Bull. Chem. Soc., Jpn.*, **45**, 450 (1972).
(15) P. C. H. Mitchell and D. A. Parker, *J. Inorg. Nucl. Chem.*, **35**, 1385 (1973).
(16) E. Munck, P. G. Debrunner, J. C. M. Tsibris, and I. C. Gunsalus, *Biochemistry*, **11**, 855 (1972).
(17) C. R. Hill and P. G. Debrunner, Physics Department, University of Illinois.
(18) J. P. Chandler, Program 66, Quantum Chemistry Program Exchange, Indiana University, Bloomington, Ind.
(19) B. L. Chrisman and T. A. Tumolillo, *Comput. Phys. Commun.*, **2**, 322 (1971).
(20) M. T. Mocella, M. S. Okamoto, and E. K. Barefield, *Synth. React. Inorg. Met.-Org. Chem.*, **4**, 69 (1974).
(21) R. D. Feltham and R. G. Hayter, *J. Chem. Soc.*, 4587 (1964).
(22) W. Wojciechowski, *Inorg. Chim. Acta*, **1**, 324 (1967).
(23) W. Wojciechowski, *Inorg. Chim. Acta*, **1**, 319 (1967).
(24) A. P. Ginsberg, R. L. Martin, R. W. Brookes, and R. C. Sherwood, *Inorg. Chem.*, **11**, 2884 (1972).
(25) T. H. Moss, H. R. Lillienthal, C. Moleski, G. A. Smythe, M. C. McDaniel, and W. S. Caughey, *J. Chem. Soc., Chem. Commun.*, 263 (1972).
(26) B. Jezowska-Trzebiatowska, H. Kozlowski, T. Cukierda, and A. Ozarowski, *J. Mol. Struct.*, **19**, 663 (1973).
(27) S. J. Gruber, C. M. Harris, and E. Sinn, *J. Inorg. Nucl. Chem.*, **30**, 1805 (1968).
(28) L. J. Boucher and C. G. Coe, *Inorg. Chem.*, **14**, 1289 (1975).
(29) R. F. Ziolo, R. H. Stanford, G. R. Rossman, and H. B. Gray, *J. Am. Chem. Soc.*, **96**, 7910 (1974).
(30) R. Grecu and D. Lupu, *Rev. Roum. Chim.*, **16**, 1811 (1971).
(31) M. B. Robin and P. Day, *Adv. Inorg. Chem. Radiochem.*, **10**, 247 (1967).
(32) G. C. Allen and N. S. Hush, *Prog. Inorg. Chem.*, **8**, 357 (1967); N. S. Hush, *ibid.*, **8**, 391 (1967).
(33) W. M. Reiff, W. A. Baker, Jr., and N. E. Erickson, *J. Am. Chem. Soc.*, **90**, 4794 (1968).
(34) W. S. Caughey, H. Eberspaecher, W. H. Fuchsman, and S. McCoy, *Ann. N.Y. Acad. Sci.*, **153**, 722 (1969).
(35) I. A. Cohen, *J. Am. Chem. Soc.*, **91**, 1980 (1969).
(36) B. Jezowska-Trzebiatowska, J. Hanuza, A. Ozarowska, and H. Kozlowskii, *Bull. Acad. Pol. Sci., Ser. Sci. Chim.*, **23**, 609 (1975).
(37) M. A. Torrens, D. K. Straub, and L. M. Epstein, *J. Am. Chem. Soc.*, **94**, 4160 (1972).
(38) C. Maricondi, D. K. Straub, and L. M. Epstein, *J. Am. Chem. Soc.*, **94**, 4157 (1972).
(39) J. Peisach, W. E. Blumberg, S. Ogawa, E. A. Rachmilewitz, and R. Oltzik, *J. Biol. Chem.*, **246**, 3342 (1971).
(40) H. J. Schugar, G. R. Rossman, and H. B. Gray, *J. Am. Chem. Soc.*, **91**, 4564 (1969).
(41) R. M. Golding and K. J. Jessop, *Aust. J. Chem.*, **28**, 179 (1975).
(42) W. M. Reiff, G. J. Long, and W. A. Baker, Jr., *J. Am. Chem. Soc.*, **90**, 6347 (1968); M. Gerloch, J. Lewis, F. E. Mabbs, and A. Richards, *J. Chem. Soc. A*, 112 (1968).
(43) G. M. Bancroft, A. G. Maddock, and R. P. Randl, *J. Chem. Soc. A*, 2939 (1968).
(44) V. McKee, S. M. Nelson, and J. Nelson, *J. Chem. Soc., Chem. Commun.*, 225 (1976).